

Magnetars as cooling neutron stars with internal heating

A. D. Kaminker,¹ D. G. Yakovlev,^{1*} A. Y. Potekhin,¹ N. Shibazaki,² P. S. Shternin¹
and O. Y. Gnedin³

¹*Ioffe Physico-Technical Institute, Politekhmicheskaya 26, 194021 Saint-Petersburg, Russia*

²*Rikkyo University, Tokyo 171-8501, Japan*

³*Ohio State University, Columbus, OH 43210, USA*

Accepted 2006 June 12. Received 2006 June 9; in original form 2006 May 18

ABSTRACT

We study thermal structure and evolution of magnetars as cooling neutron stars with a phenomenological heat source in a spherical internal layer. We explore the location of this layer as well as the heating rate that could explain high observable thermal luminosities of magnetars and would be consistent with the energy budget of neutron stars. We conclude that the heat source should be located in an outer magnetar's crust, at densities $\rho \lesssim 5 \times 10^{11} \text{ g cm}^{-3}$, and should have the heat intensity of $\sim 10^{20} \text{ erg cm}^{-3} \text{ s}^{-1}$. Otherwise the heat energy is mainly emitted by neutrinos and cannot warm up the surface.

Key words: dense matter – neutrinos – stars: magnetic fields – stars: neutron.

1 INTRODUCTION

There is growing evidence that soft gamma-ray repeaters (SGRs) and anomalous X-ray pulsars (AXPs) belong to the same class of objects, *magnetars*, which are warm, isolated, slowly rotating neutron stars of age $t \lesssim 10^5 \text{ yr}$ with unusually strong magnetic fields, $B \gtrsim 10^{14} \text{ G}$ (see e.g. Woods & Thompson 2006, for a recent review). There have been attempts to explain the activity of these sources and the high level of their X-ray emission by the release of the magnetic energy in their interiors, but a reliable theory is still absent.

In this paper, we analyse the thermal evolution of magnetars as cooling isolated neutron stars. We do not attempt to construct a self-consistent theory of the magnetars but instead address the problem phenomenologically. We show that magnetars are too hot to be treated as purely cooling neutron stars; they require some heating source, which we assume operates in their interiors. Our aim is to analyse the location and power of the heating source that are consistent with observed thermal luminosities of SGRs and AXPs and with the energy budget of an isolated neutron star.

2 PHYSICS INPUT

We use our general relativistic cooling code (Gnedin, Yakovlev & Potekhin 2001). It simulates the thermal evolution of an initially hot isolated neutron star taking into account heat outflow via neutrino emission from the star and via thermal conduction within the star, with subsequent thermal photon emission from the surface. To facilitate calculations, the star is artificially divided (e.g. Gudmundsson, Pethick & Epstein 1983) into a thin outer heat-blanketing envelope

(extending from the surface to the layer of density $\rho = \rho_b \sim 10^{10} - 10^{11} \text{ g cm}^{-3}$, with the thickness of a few hundred metres) and the bulk interior (from ρ_b to the centre). In the bulk interior, the code solves the full set of equations of thermal evolution in the spherically symmetric approximation, neglecting the effects of magnetic fields on thermal conduction and neutrino emission. In the blanketing envelope, the code uses the solution of the stationary thermal conduction problem obtained in the approximation of a thin plane-parallel layer for a dipole magnetic field configuration. This solution relates temperature T_b at the base of the blanketing envelope ($\rho = \rho_b$) to the effective surface temperature T_s properly averaged over the neutron star surface (e.g. Potekhin & Yakovlev 2001; Potekhin et al. 2003).

In the code, we have mainly used the $T_b - T_s$ relation obtained specifically for the present study, assuming $\rho_b = 10^{10} \text{ g cm}^{-3}$ and the magnetized blanketing envelope is made of iron. Magnetars are hot and have large temperature gradients extending deeply into the heat blanketing envelope. Thus even high magnetic fields do not dramatically affect the overall thermal conduction in the envelope or the $T_b - T_s$ relation (as discussed, e.g., by Potekhin et al. 2003). An anisotropy of heat conduction, induced by the magnetic field in a hot magnetar crust, is expected to be insufficiently high to greatly modify the temperature distribution in the bulk of the star ($\rho > \rho_b$) and to create strong deviations of this distribution from spherical symmetry (see Section 4.1). At lower temperatures, the anisotropy would be much stronger and this statement would be more questionable (Geppert, Küker & Page 2004, 2006). Our standard cooling code includes the effects of magnetic fields only in the blanketing envelope. In this respect, our present model of the blanketing envelope with $\rho_b = 10^{10} \text{ g cm}^{-3}$ seems less adequate than the previous model with $\rho_b = 4 \times 10^{11} \text{ g cm}^{-3}$ (Potekhin et al. 2003). However, the blanketing models, by construction, neglect neutrino emission from the blanketing envelope. Because the

*E-mail: yak@astro.ioffe.ru

neutrino emission from the layers with $\rho \gtrsim 3 \times 10^{10} \text{ g cm}^{-3}$ in hot magnetars is important (Section 3), the blanketing envelope with $\rho_b = 10^{10} \text{ g cm}^{-3}$ is expected to be more appropriate for the present investigation. That is why we have performed calculations with this latter model but have done additional tests using the model with $\rho_b = 4 \times 10^{11} \text{ g cm}^{-3}$ (Section 4.1).

We have also included, in a phenomenological manner, the effects of magnetic fields on the thermal evolution of the bulk stellar interior. Most importantly, we have introduced a heat source located within a spherical layer in the interior (it can be associated with the magnetic field; Section 4.2). The heating rate H ($\text{erg cm}^{-3} \text{ s}^{-1}$) has been taken in the form

$$H = H_0 \Theta(\rho_1, \rho_2) \exp(-t/\tau), \quad (1)$$

where H_0 is the maximum heat intensity, $\Theta(\rho_1, \rho_2)$ is a step-like function ($\Theta \approx 1$ within the density interval $\rho_1 < \rho < \rho_2$; $\Theta \approx 0$ outside this interval, with a sharp but continuous transitions at the interval boundaries), t is the star's age and τ is the lifetime of the heating source. A specific form of H is not important for our main conclusions. We do not specify the nature of this source. We set $\tau = 5 \times 10^4 \text{ yr}$ to explain high thermal states of all observed SGRs and AXPs (Section 3). We do not consider longer τ which would require higher energy budget (while the budget is already severely restricted even for $\tau = 5 \times 10^4 \text{ yr}$). We treat H_0 , ρ_1 and ρ_2 as free parameters with the aim to understand what the intensity and the location of the heat source should be in order to be consistent with observations and with the energy budget of an isolated neutron star.

It is instructive to introduce the total heat power W^∞ (erg s^{-1}), redshifted for a distant observer,

$$W^\infty(t) = \int dV e^{2\Phi} H, \quad (2)$$

where dV is the proper volume element and Φ is the redshift metric function.

In the neutron star core, we use the equation of state of dense matter constructed by Akmal, Pandharipande & Ravenhall (1998) (model Argon V18 + δv + UIX*); it is currently considered the most elaborated equation of state of neutron star matter. Specifically, we employ a convenient parametrization of this equation of state proposed by Heiselberg & Hjorth-Jensen (1999) and described as APR III by Gusakov et al. (2005). According to this equation of state, neutron star cores consist of neutrons, protons, electrons and muons. The maximum (gravitational) neutron star mass is $M = 1.929 M_\odot$. The powerful direct Urca process of neutrino emission (Lattimer et al. 1991) is allowed only in the central kernels of massive neutron stars with $M > 1.685 M_\odot$ (at densities $\rho > 1.275 \times 10^{15} \text{ g cm}^{-3}$).

We use neutron star models with two masses, $M = 1.4$ and $1.9 M_\odot$. The $1.4 M_\odot$ model is an example of a star with standard (not too strong) neutrino emission in the core (provided by the modified Urca process in a non-superfluid star). In this case, the (circumferential) stellar radius is $R = 12.27 \text{ km}$, and the central density is $\rho_c = 9.280 \times 10^{14} \text{ g cm}^{-3}$. The $1.9 M_\odot$ model ($R = 10.95 \text{ km}$, $\rho_c = 2.050 \times 10^{15} \text{ g cm}^{-3}$) is an example of a star whose neutrino emission is enhanced by the direct Urca process in the inner core.

We have updated the thermal conductivity of electrons and muons in the stellar core by new results (Shternin & Yakovlev, in preparation) which take into account the Landau damping of transverse plasmons in the interaction of electrons and muons with surrounding charged particles (following the results for quark plasma obtained by Heiselberg & Pethick 1993). This update has not notably affected our cooling scenarios.

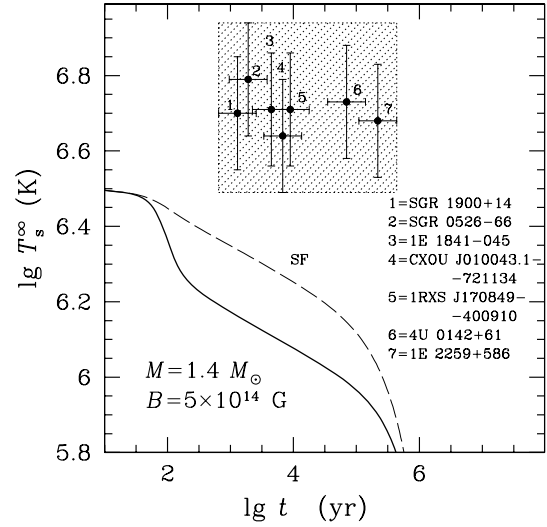


Figure 1. Observational data on the blackbody surface temperatures T_s^∞ of seven magnetars. The shaded rectangle is the ‘magnetar box’. The data are compared to the theoretical cooling curves of the $1.4 M_\odot$ neutron star with $B = 5 \times 10^{14} \text{ G}$ and no internal heating, either without superfluidity (the solid line) or with strong proton superfluidity in the core (the dashed line SF).

3 RESULTS

For the observational basis, we take seven sources (two SGRs and five AXPs, indicated in Fig. 1). The estimates of their spindown ages t , surface magnetic fields B and the blackbody surface temperatures T_s^∞ (redshifted for a distant observer) are taken from tables 14.1 and 14.2 of the review paper by Woods & Thompson (2006) and from the paper by McGarry et al. (2005). The data are from the original publications of Kulkarni et al. (2003) (SGR 0526–66); Woods et al. (2001, 2002) (SGR 1900+14); Gotthelf et al. (2002) and Morii et al. (2003) (1E 1841–045); McGarry et al. (2005) (CXOU J010043.1–721134); Gavriil & Kaspi (2002) and Rea et al. (2003) (1RXS J170849–400910); Gavriil & Kaspi (2002) and Patel et al. (2003) (4U 0142+61); Gavriil & Kaspi (2002) and Woods et al. (2004) (1E 2259+586). In the absence of T_s^∞ estimates for SGR 1627–41, we do not include this SGR in our analysis. We have also excluded SGR 1806–20 and several AXPs whose thermal emission component and characteristic age seem less certain. The radiation from the selected sources has the pulsed fraction $\lesssim 20$ per cent, and for some of them the pulsed fraction is $\lesssim 10$ per cent. This may indicate that the thermal radiation can be emitted from a substantial part of the surface (although the pulsed fraction can also be lowered by the gravitational lensing effect).

The blackbody surface temperatures T_s^∞ of the selected sources are plotted in Fig. 1 versus spindown ages t . Woods & Thompson (2006) present these data without formal errors, which are actually large. We introduce, somewhat arbitrarily, the 30 per cent uncertainties into the values of T_s^∞ and the uncertainties by a factor of 2 into the values of t . The data are too uncertain and our cooling models are too simplified to explain every source by its own cooling model. Instead, we try to explain the existence of magnetars as cooling neutron stars that belong to the ‘magnetar box’, the shaded rectangle in Fig. 1 (attributed to an average persistent thermal emission from magnetars, excluding bursting states). Our results will be sufficiently insensitive to the neutron star mass, and we will mainly use the neutron star model with $M = 1.4 M_\odot$ (unless the contrary is

indicated). Similarly, the results will not be too sensitive to superfluid state of stellar interiors, and we will mostly neglect the effects of superfluidity of nucleons in the stellar crust and core. To be specific, we mainly assume the dipole magnetic field in the blanketing envelope with $B = 5 \times 10^{14}$ G at the magnetic poles. Some variations of B will not affect our principal conclusions (Section 4.1).

In Fig. 1, we show the theoretical cooling curves $T_s^\infty(t)$ for the $1.4\text{-}M_\odot$ isolated magnetized neutron star without any internal heating. The solid line refers to a non-superfluid neutron star, while the dashed line, labelled ‘SF’, is for strong proton superfluidity in the stellar core. This superfluidity strongly suppresses neutrino emission in the core and notably increases T_s^∞ at the neutrino cooling stage (e.g. Yakovlev & Pethick 2004). Let us stress that the surface temperature of these stars is highly non-uniform, with the magnetic poles being much hotter than the equator. In the figures, we plot the average surface temperature (e.g. Potekhin et al. 2003). Clearly, the magnetars are much hotter than ordinary cooling neutron stars. The observations of ordinary neutron stars can be explained by the cooling theory without any reheating (e.g. Yakovlev & Pethick 2004; Page, Geppert & Weber 2006), while the observations of magnetars suggest that the magnetars have additional heat sources. We assume further that these sources are located inside magnetars. According to alternative models, powerful energy sources can be available in magnetar magnetospheres (Thompson & Beloborodov 2005; Beloborodov & Thompson 2006).

We introduce the internal sources in a phenomenological way described in Section 2. All results presented below (Figs 2–5) are obtained including the internal heating in accordance with equation (1). They indicate that the magnetars are hot inside, with the temperature $T \sim 10^9$ K (or even higher) in the crust, at $\rho \gtrsim 3 \times 10^{10}$ g cm $^{-3}$. Such stars are very strong sources of neutrino emission, which is vitally important for the magnetar thermal structure and evolution.

Our simulations of cooling neutron stars with a powerful internal heating show that after a short initial relaxation ($t \lesssim 10$ yr) the star reaches a quasi-stationary state, which is fully determined by the heating source. The energy is mainly carried away by neutrinos, but some fraction is transported by thermal conduction to the surface and radiated away by photons. The interior of these cooling neutron stars is highly non-isothermal. The hotter layers are those where the heat is released and the neutrino emission is not too strong; these layers are located in the crust. The approximation of isothermal

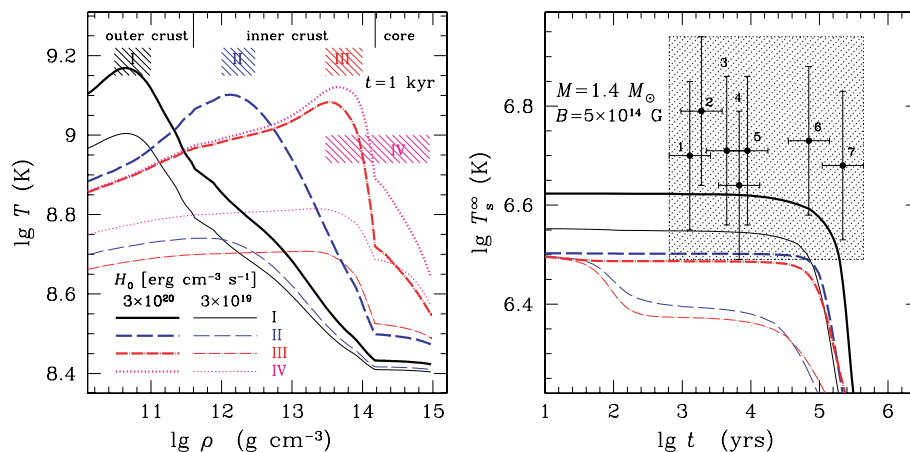


Figure 2. Left-hand panel: temperature profiles within the $1.4 M_\odot$ neutron star of age $t = 1000$ yr with four different positions I–IV of the heating layer (given in Table 1 and indicated by hatched rectangles) and two levels of the heat intensity $H_0 = 3 \times 10^{19}$ and 3×10^{20} erg cm $^{-3}$ s $^{-1}$. The magnetic field is $B = 5 \times 10^{14}$ G. Right-hand panel: cooling curves for these models compared with the observations.

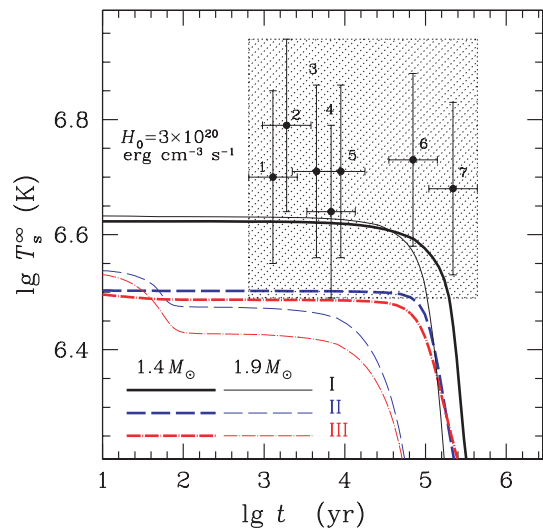


Figure 3. Same as in the right-hand panel of Fig. 2 for the three positions of the heating layer, one value of the heat intensity and two neutron star masses, 1.4 and $1.9 M_\odot$.

interior, which is excellent for ordinary middle-aged neutron stars, cannot be used while studying the cooling of magnetars.

The left-hand panel of Fig. 2 shows the temperature distribution inside the $1.4\text{-}M_\odot$ star of age $t = 1000$ yr. This distribution remains the same during the entire magnetar stage ($t \lesssim \tau$, see equation 1), and we have chosen $t = 1000$ yr just as an example. We have considered four locations of the heat layer, $\rho_1 - \rho_2$, summarized in Table 1: (I) 3×10^{10} – 10^{11} g cm $^{-3}$ (in the outer crust, just below the heat blanketing envelope), (II) 10^{12} – 3×10^{12} g cm $^{-3}$ (at the top of the inner crust), (III) 3×10^{13} – 10^{14} g cm $^{-3}$ (at the bottom of the inner crust) and (IV) 3×10^{13} – 9×10^{14} g cm $^{-3}$ (at the bottom of the inner crust and in the entire core). These locations are marked by hatched rectangles. The density ranges, which are appropriate to the outer crust, the inner crust and the core, are indicated in the upper part of the figure. Let us remind the reader that the outer crust has a thickness of a few hundred metres and a mass of $\sim 10^{-5} M_\odot$, the inner crust can be as thick as 1 km and its mass is $\sim 10^{-2} M_\odot$, while the core is large (radius ~ 10 km) and contains ~ 99 per cent of the stellar mass. Therefore, the heating layers I, II and III are

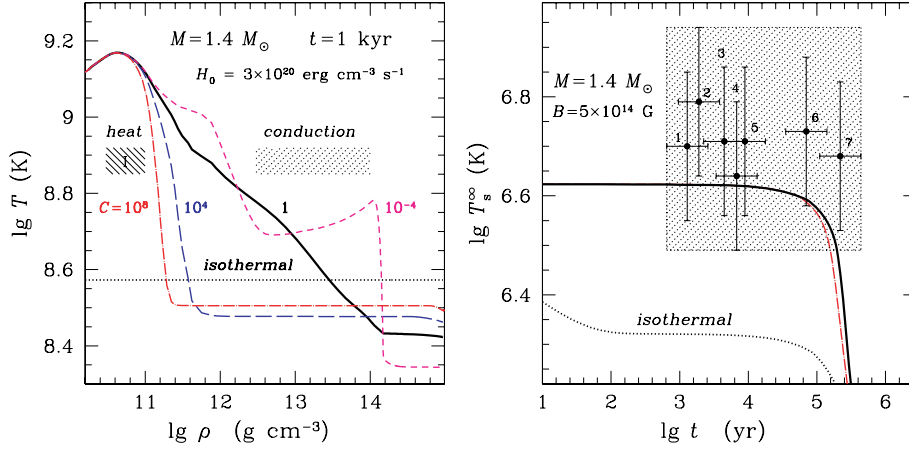


Figure 4. The effect of the thermal conductivity in the inner crust on the thermal evolution of the $1.4\text{-}M_{\odot}$ magnetar with the heating layer I and the heat intensity $H_0 = 3 \times 10^{20} \text{ erg cm}^{-3} \text{ s}^{-1}$. Left-hand panel: the temperature profiles within the magnetar at $t=1000$ yr. The hatched rectangles show the positions of the heating layer and the layer where the thermal conductivity was modified. Right-hand panel: the cooling curves. The thick solid lines are the same as in Fig. 2. Thinner long-dashed, dot-dashed and short-dashed lines are for the star with the thermal conductivity modified by a factor of $C = 10^4, 10^8$ and 10^{-4} , respectively, in the density range from 3×10^{12} to $10^{14} \text{ g cm}^{-3}$. The dotted line marked *isothermal* is for an infinite thermal conductivity in the star bulk ($\rho > 10^{10} \text{ g cm}^{-3}$).

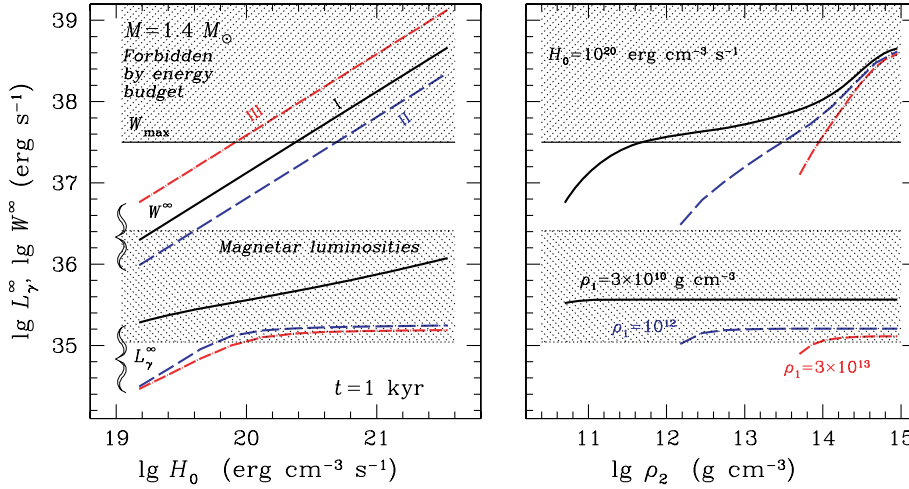


Figure 5. The total heat power W^{∞} (higher curves) and the surface photon luminosity L_{γ}^{∞} (lower curves) versus parameters of the heating layer compared to the values of L_{γ}^{∞} from the ‘magnetar box’ (the lower shaded strip) and to the values of W^{∞} forbidden by energy budget (the upper shading) for the $1.4\text{-}M_{\odot}$ neutron star of age 1000 yr. Left-hand panel: three fixed positions of the heating layer of variable heat intensity H_0 . Right-hand panel: three fixed minimum densities ρ_1 of the heating layer, the fixed heat intensity $H_0 = 10^{20} \text{ erg cm}^{-3} \text{ s}^{-1}$ and variable maximum density ρ_2 .

Table 1. Four positions of the heating layer, and the heating power W^{∞} for the $1.4\text{-}M_{\odot}$ star with $H_0 = 3 \times 10^{20} \text{ erg cm}^{-3} \text{ s}^{-1}$ and $t = 1$ kyr.

No.	$\rho_1 (\text{g cm}^{-3})$	$\rho_2 (\text{g cm}^{-3})$	$W^{\infty} (\text{erg s}^{-1})$
I	3×10^{10}	10^{11}	4.0×10^{37}
II	10^{12}	3×10^{12}	1.9×10^{37}
III	3×10^{13}	10^{14}	1.1×10^{38}
IV	3×10^{13}	9×10^{14}	1.1×10^{39}

relatively thin, while the heating layer IV is wide and includes most of the stellar volume. We have allowed our heat sources to have two different intensities, $H_0 = 3 \times 10^{19}$ and $3 \times 10^{20} \text{ erg cm}^{-3} \text{ s}^{-1}$. For illustration, in Table 1 we present also the heating power W^{∞} calculated from equation (2) for the four layers in the $1.4\text{-}M_{\odot}$ star of age $t = 1000$ yr at $H_0 = 3 \times 10^{20} \text{ erg cm}^{-3} \text{ s}^{-1}$.

In all the cases, the neutron star core appears to be much colder than the crust because the core quickly cools down via strong neutrino emission (via the modified Urca process for the conditions in Fig. 2). Placing the heat sources far from the heat blanketing envelope is an inefficient way to maintain warm surface; the heating layer can be hot, but the energy is radiated away by neutrinos and does not flow to the surface. For the deep heating layers (cases II, III or IV), the heat intensity $H_0 = 3 \times 10^{19} \text{ erg cm}^{-3} \text{ s}^{-1}$ is clearly insufficient to warm the surface to the magnetar level. The higher intensity $3 \times 10^{20} \text{ erg cm}^{-3} \text{ s}^{-1}$ helps but is still less efficient in these layers than in layer I, which is close to the heat blanketing envelope. For the latter H_0 the heating of the crust bottom (case III) and the heating of the entire core (case IV) lead to the same surface temperature of the star. Thus, the most efficient way to warm the surface is to place the heating layer in the outer crust, near the heat blanketing envelope. This conclusion is further supported by Figs 3–5.

The right-hand panel of Fig. 2 shows cooling curves of the $1.4\text{-}M_{\odot}$ stars for the same models of the heating layer as in the left-hand panel (with one exception – we do not show the cooling curves for the case IV, for simplicity). The cooling curves of the star of age $t \lesssim 5 \times 10^4$ yr are almost horizontal, indicating that these stars maintain their high thermal state owing to the internal heating. Non-horizontal initial parts ($t \lesssim 100$ yr) of two curves, which correspond to deep and non-intense heating, show the residual initial relaxation to quasi-stationary thermal states. One can see that the only way to explain the sources from the ‘magnetar box’ is to place the heating source in the outer crust and assume $H_0 \sim 10^{20}$ erg cm^{-3} s^{-1} . As the heating is exponentially switched off at $t \gtrsim 5 \times 10^4$ yr, following equation (1), the surface temperature drops down accordingly. The magnetar stage is over and the star transforms into the ordinary cooling neutron star (Potekhin et al. 2003) which cools mainly via the surface photon emission.

Fig. 3 compares cooling curves of neutron stars of two masses, 1.4 and $1.9 M_{\odot}$, for the same three locations I–III of the heating layer and for one heat intensity $H_0 = 3 \times 10^{20}$ erg cm^{-3} s^{-1} . The thick lines are for the $1.4\text{-}M_{\odot}$ star; they are the same as in the right-hand panel of Fig. 2. The thin lines are the respective curves for the $1.9\text{-}M_{\odot}$ star, which is a very efficient neutrino emitter because of the direct Urca process in its core (Section 2). If the heating layer is in the location II or III (in the inner crust), the enhanced neutrino emission from the core of the massive star carries away a substantial amount of heat and decreases the surface temperature of the star. If, however, the heating layer is placed in the outer crust (case I), direct Urca in the core has almost no effect on the surface temperature. In this case, the surface temperature is almost insensitive to the physical conditions in the stellar core and in the inner crust, in particular, to the neutrino emission mechanisms and superfluid state of matter. In other words, surface layers are thermally decoupled from the deep interior. A similar situation occurs in ordinary young and hot cooling stars in the initial cooling stage, before internal thermal relaxation (Lattimer et al. 1994; Gnedin et al. 2001). This justifies our neglect of the effects of superfluidity in the calculations (although these effects can be vitally important for ordinary middle-aged cooling neutron stars; e.g. Yakovlev & Pethick 2004; Page et al. 2006).

Fig. 4 demonstrates sensitivity of the results to the values of the thermal conductivity in the inner neutron star crust. It shows temperature profiles in the $1.4\text{-}M_{\odot}$ star of age 1000 yr and the cooling curves of this star for one location of the heating layer (case I) and one heat intensity $H_0 = 3 \times 10^{20}$ erg cm^{-3} s^{-1} . The thick lines are the same as in Fig. 2. They are calculated with our standard cooling code assuming only electron thermal conductivity in the crust (Gnedin et al. 2001). However, in the inner crust thermal energy can also be transported by free neutrons and this transport can be very efficient, especially if neutrons are in a superfluid state. The effect may be similar to that in superfluid ${}^4\text{He}$, where no temperature gradients can be created in laboratory experiments because they are immediately smeared out by responding convective flows (e.g. Tilley & Tilley 1990). To simulate this effect, we have artificially introduced the layer of high thermal conductivity in the inner neutron star crust, in the density range from 3×10^{12} to 10^{14} g cm^{-3} . In this layer, we enhanced the thermal conductivity by a factor of $C = 10^4$ or 10^8 . These values of C are arbitrary (taken for illustration). The enhancement changes dramatically the temperature profiles in the inner crust, making it much cooler and almost isothermal. We have also made one test run by reducing the thermal conductivity in the indicated layer by a factor of 10^4 . This corresponds to $C = 10^{-4}$ and mainly increases the temperature in the inner crust. Such a strong conductivity reduction is also artificial and illustra-

tive (it may reflect a great suppression of radial heat conduction in the inner crust with a strong toroidal magnetic field). However, all these strong changes of the temperature profiles in the inner crust have almost no effect on the surface temperature and the cooling curves. It is another manifestation of the thermal decoupling of the surface layers from the inner parts of the star. In addition, we have simulated the cooling of the star (the dotted curves) in the approximation of infinite thermal conductivity everywhere in the star bulk ($\rho > \rho_b = 10^{10}$ g cm^{-3}). In this case, the heat energy is instantly spread over the star bulk, which makes the stellar surface much cooler than in the case of finite conduction.

Fig. 5 shows the integrated heating rate W^{∞} , given by equation (2) (three upper lines in each panel), and the photon thermal surface luminosity of the star L_{γ}^{∞} (redshifted for a distant observer, three lower lines in each panel) as a function of parameters of the heating layers. The results are presented for the $1.4\text{-}M_{\odot}$ star of age 1000 yr.

In the left-hand panel, we select three locations of the heating layer (I, II and III) and vary the heat intensity H_0 . One can clearly see that only the heating layer I can produce $L_{\gamma}^{\infty} \gtrsim 3 \times 10^{35}$ erg s^{-1} , typical for magnetars. Moreover, the surface luminosity increases with H_0 much slower than the heating rate. For $H_0 \gtrsim 10^{20}$ erg cm^{-3} s^{-1} and the layers II and III, the luminosity is seen to saturate. This means that *pumping additional heat energy into the heating layer does not affect L_{γ}^{∞}* . The efficiency of converting the input heat into the surface radiation ($L_{\gamma}^{\infty}/W^{\infty}$) is generally small. The highest efficiency is achieved if we heat the outer crust (layer I) with low intensity.

In the right-hand panel of Fig. 5, we present L_{γ}^{∞} and W^{∞} as a function of the maximum density ρ_2 of the heating layer, for one heat intensity $H_0 = 10^{20}$ erg cm^{-3} s^{-1} and three fixed minimum densities of this layer ($\rho_1 = 3 \times 10^{10}$, 10^{12} and 3×10^{13} g cm^{-3}). One can observe the saturation of L_{γ}^{∞} with increasing ρ_2 . If ρ_2 is large and the heating layer is extended into the core, the heat energy is huge. However, as long as ρ_1 is far from the surface, this huge energy is almost fully carried away by neutrinos and does not heat the surface. In this case, the efficiency of heat conversion into the surface emission is very low.

In Fig. 5, we compare qualitatively the calculated values of L_{γ}^{∞} with the thermal surface luminosities from the ‘magnetar box’ (the lower shaded strip, estimated using accepted values of T_s^{∞} and the $1.4\text{-}M_{\odot}$ neutron star model). The heating should be sufficiently intense to raise L_{γ}^{∞} to these magnetar values. It is the first requirement to explain the observations of the magnetars. The second requirement stems from the energy budget of an isolated neutron star. The heat energy is assumed to be taken from some source which pumps the energy W^{∞} into the heating layer during magnetar’s life ($\tau \sim 5 \times 10^4$ yr in equation 1). Naturally, the total available energy E_{tot} is restricted. At least it should be much smaller than $\sim 5 \times 10^{53}$ erg, the gravitational energy of the neutron star. We assume that the maximum energy of the internal heating is $E_{\text{max}} \sim 10^{50}$ erg (which is the magnetic energy of the star with the magnetic field $B = 3 \times 10^{16}$ G in the core). Then the maximum energy generation rate is $W_{\text{max}} \sim E_{\text{max}}/\tau \sim 3 \times 10^{37}$ erg s^{-1} , which is plotted by the upper horizontal solid line in Fig. 5. The upper shaded space above this line is thus prohibited by the energy budget.

A successful interpretation of magnetars as cooling neutron stars requires L_{γ}^{∞} to be sufficiently high to reach the ‘magnetar box’ and W^{∞} to be sufficiently low to avoid the prohibited region. These conditions are fulfilled for the heating layer located in the outer stellar crust and the heat intensities H_0 between 3×10^{19} and 3×10^{20} erg cm^{-3} s^{-1} (higher value preferred). A typical efficiency of heat conversion into the surface emission under these conditions is $L_{\gamma}^{\infty}/W^{\infty} \sim 10^{-2}$.

4 DISCUSSION

4.1 Testing the results

We have performed a number of additional tests. In particular, we have studied sensitivity of our results to the values of the neutrino emissivity in the neutron star core and crust. We find that variations of the neutrino emissivity in the inner crust and the core of the star that undergoes intense heating can strongly affect the temperature profiles in the stellar interior but have almost no effect on the surface temperature. This is another example of the thermal decoupling of the outer crust and deep interiors. On the other hand, we find that L_{ν}^{∞} is sensitive to the neutrino emission in the outer crust. This emission in a hot crust is mainly generated by plasmon decay and electron–nucleus bremsstrahlung mechanisms (see, e.g. Yakovlev et al. 2001). If magnetars have very strong magnetic fields in their outer crusts, these fields can greatly modify the plasmon decay neutrino process. Such modifications have not been studied in detail but can be important for the magnetar physics.

We have made some test runs taking into account the effects of superfluidity. In particular, we have included superfluidity of free neutrons in the inner crust and the associated neutrino emission via Cooper pairing of neutrons. This neutrino emission affects the temperature profiles in the inner crust but has almost no effect on the surface temperature.

We have also varied the maximum density ρ_b of the heat blanketing layer, shifting it from the present position $\rho_b = 10^{10}$ (Section 2) to 4×10^{11} g cm $^{-3}$, as in our previous model (Potekhin et al. 2003). In addition, we have varied the magnetic field strength B in the blanketing envelope from $B = 5 \times 10^{13}$ to 5×10^{15} G. The cooling curves and the internal temperature profiles are sensitive to these variations but do not violate our principal conclusions.

Let us recall that we have neglected the effects of the magnetic field on heat transport in the star’s bulk (Section 2). The main effect is the anisotropy of electron thermal conduction described by the electron magnetization parameter $\omega_e \tau_e$, where ω_e is the electron gyrofrequency and τ_e is an effective electron relaxation time (see e.g. Geppert et al. 2004, and references therein). For typical conditions in Fig. 4, we have $\omega_e \tau_e \lesssim 30$ in the magnetar’s crust. As follows from the results of Geppert et al. (2004, 2006) (obtained for colder neutron stars, where neutrino emission from the crust was unimportant), such values of $\omega_e \tau_e$ are insufficiently high to change dramatically the overall temperature distribution in the crust. We expect that the temperature distribution in a hot magnetar crust is more strongly affected by intense neutrino emission than by heat conduction anisotropy. It would be desirable to reconsider the cooling of magnetars with a more careful treatment of heat transport and neutrino emission in the magnetized outer crust.

4.2 The nature of internal heating

The development of a specific theoretical model of the internal heating is outside the scope of this paper (existing models are summarized, e.g. in review papers by Woods & Thompson 2006 and Heyl 2006). Nevertheless, our results place stringent constraints on the possible models. The main requirement is that the total heat energy should be huge, $E_{\text{tot}} \sim 10^{49}–10^{50}$ erg, and should be released during $10^4–10^5$ yr in the outer neutron star crust. This does not necessarily require that the energy is stored in the outer crust but it is effectively transformed into heat there.

Our results agree with the widespread point of view that the magnetars cannot be powered by their rotation, accretion, the thermal

energy in a cooling star or the strain energy accumulated in the crust. All these energy sources contain much less than 10^{49} erg.

Nevertheless, the required energy can be accumulated in the magnetic field if, for example, the star possesses the field $B \sim (1–3) \times 10^{16}$ G in its core. The evolution of this magnetic field can be accompanied by a strong energy release in the outer crust, where the electric conductivity is especially low and the field undergoes the strongest Ohmic dissipation. An actual structure of the magnetic field in the star can be complicated. In particular, the magnetic configuration in the crust can strongly deviate from a magnetic dipole. This complicated magnetic configuration can further enhance the Ohmic dissipation in the outer crust. There may be other mechanisms of converting the magnetic energy into heat in the outer crust. For instance, rearrangements of the internal magnetic field during the evolution of a magnetar may be accompanied by the generation of waves (perturbations) emerging from the stellar interior and dissipating in the outer crust. Some wave generation mechanisms are discussed by Thompson & Duncan (1996).

One cannot exclude that thermal radiation of magnetars is emitted from a smaller part of the neutron star surface (e.g. from hot spots near magnetic poles), implying lower total heat energies. Nevertheless, observable thermal X-ray luminosities of magnetars $\sim 10^{34}–10^{36}$ erg s $^{-1}$ (e.g. Mereghetti et al. 2002; Kaspi & Gavriil 2004; Woods & Thompson 2006) are consistent with the interval of thermal luminosities in Fig. 5 calculated assuming the emission from the entire surface.

Let us also note alternative theories of magnetars, mentioned in Section 3. These theories suggest (e.g. Beloborodov & Thompson 2006) that the main energy release occurs in the magnetar’s magnetosphere and the radiation spectrum is formed there as a result of comptonization and reprocessing of the quasi-thermal spectrum.

5 CONCLUSIONS

We have modelled thermal states and thermal evolution of magnetars (SGRs and AXPs) with the aim to explain high surface temperatures of these neutron stars and their energy budget. Our main conclusions are as follows.

(i) It is impossible to explain high thermal states of magnetars as cooling neutron stars without assuming that they undergo powerful heating. We have developed the idea that the heat source operates in the interior of magnetars.

(ii) The heat source can be located in a thin layer at densities $\rho \lesssim 5 \times 10^{11}$ g cm $^{-3}$ in the outer magnetar crust, with the heat intensity ranged from $\sim 3 \times 10^{19}$ to 3×10^{20} erg cm $^{-2}$ s $^{-1}$. The source cannot be located deeper in the interior because the heat energy would be radiated away by neutrinos; it would be unable to warm up the surface. This deeper heating is extremely inefficient and inconsistent with the energy budget of neutron stars. Pumping huge heat energy into the deeper layers would not increase the surface temperature.

(iii) Heating of the outer crust produces a strongly non-uniform temperature distribution within the star. The temperature in the heating layer exceeds 10^9 K, while the bottom of the crust and the stellar core remain much colder. The thermal state of the heat layer and of the surface is almost independent of physical parameters of deeper layers (such as the equation of state, neutrino emission, heat transport, superfluidity of baryons), which means thermal decoupling of the outer crust from the inner layers. The total energy released in the heat layer during magnetar’s life ($\sim 10^4–10^5$ yr) cannot be lower than $10^{49}–10^{50}$ erg; maximum 1 per cent of this energy can be spent to heat the surface.

The present calculations can be improved by a more careful treatment of heat conduction in a magnetized plasma of the outer crust, at $\rho > 10^{10} \text{ g cm}^{-3}$, as well as by considering different magnetic fields and the presence of light (accreted) elements in the surface layers of magnetars. We intend to study these effects in our next publication.

The nature and the physical model of internal heating are still not clear; they should be elaborated in the future. In any case, one should bear in mind that the heat energy released within the magnetars should be at least two orders of magnitude higher than the photon thermal energy emitted through their surface, and the energy release should take place in the outer stellar crust. These model-independent conclusions are consequences of the well-known principle that any hot, dense matter in stellar objects is a strong source of neutrino emission.

ACKNOWLEDGMENTS

We are grateful to U. M. R. E. Geppert, the referee of this paper, and also to V. D. Pal'shin, G. G. Pavlov, Yu. A. Shibano, V. A. Urpin and J. Ventura for their fruitful discussions and critical remarks. This work was partly supported by the Russian Foundation for Basic Research (grants 05-02-16245 and 05-02-22003), the Federal Agency for Science and Innovations (grant NSh 9879.2006.2), the Rikkyo University Invitee Research Associate Program and the Dynasty Foundation.

REFERENCES

- Akmal A., Pandharipande V. R., Ravenhall D. G., 1998, *Phys. Rev. C*, 58, 1804
 Beloborodov A. M., Thompson C., 2006, *ApJ*, submitted (astro-ph/0602417)
 Gavriil F. P., Kaspi V. M., 2002, *ApJ*, 567, 1067
 Geppert U., Küker M., Page D., 2004, *A&A*, 426, 267
 Geppert U., Küker M., Page D., 2006, *A&A*, submitted (astro-ph/0512530)
 Gnedin O. Y., Yakovlev D. G., Potekhin A. Y., 2001, *MNRAS*, 324, 725
 Gotthelf E. V., Gavriil F. P., Kaspi V. M., Vasisht G., Chakrabarty D., 2002, *ApJ*, 564, L31
 Gudmundsson E. H., Pethick C. J., Epstein R. I., 1983, *ApJ*, 272, 286
 Gusakov M. E., Kaminker A. D., Yakovlev D. G., Gnedin O. Y., 2005, *MNRAS*, 363, 555

- Heiselberg H., Hjorth-Jensen M., 1999, *ApJ*, 525, L45
 Heiselberg H., Pethick C. J., 1993, *Phys. Rev. D*, 48, 2916
 Heyl J., 2006, in Chen P., Bloom E., Madejski G., Petrosian V., eds, *Proc. XXII Texas Symp. Relativistic Astrophysics*. In press (astro-ph/0504077)
 Kaspi V. M., Gavriil F. P., 2004, *Nucl. Phys. B*, 132, 456
 Kulkarni S. R., Kaplan D. L., Marshall H. L., Frail D. A., Murakami T., Yonetoku D., 2003, *ApJ*, 585, 948
 Lattimer J. M., Pethick C. J., Prakash M., Haensel P., 1991, *Phys. Rev. Lett.*, 66, 2701
 Lattimer J. M., Van Riper K. A., Prakash M., Prakash M., 1994, *ApJ*, 425, 802
 McGarry M. B., Gaensler B. M., Ransom S. M., Kaspi V. M., Veljkovic S., 2005, *ApJ*, 627, L137
 Mereghetti S., Chiarlone L., Israel G. L., Stella L., 2002, in Becker W., Lesch H., Trümper J., eds, *MPE Report 278, 270 WE-Heraeus Seminar on Neutron Stars, Pulsars and Supernova Remnants*. Max Plank Institut für Extraterrestrische Physik, Garching, p. 29
 Morii M., Sato R., Kataoka J., Kawai N., 2003, *PASJ*, 55, L45
 Page D., Geppert U., Weber F., 2006, *Nucl. Phys.*, in press (astro-ph/0508056)
 Patel S. K. et al., 2003, *ApJ*, 587, 367
 Potekhin A. Y., Yakovlev D. G., 2001, *A&A*, 374, 213
 Potekhin A. Y., Yakovlev D. G., Chabrier G., Gnedin O. Y., 2003, *ApJ*, 594, 404
 Rea N., Israel G. L., Stella L., Oosterbroek T., Mereghetti S., Angelini L., Campana S., Covino S., 2003, *ApJ*, 586, L65
 Thompson C., Beloborodov A. M., 2005, *ApJ*, 634, 565
 Thompson C., Duncan R. C., 1996, *ApJ*, 473, 322
 Tilley D. R., Tilley J., 1990, *Superfluidity and Superconductivity*. IOP Publishing, Bristol
 Woods P. M., Thompson C., 2006, in Lewin W. H. G., van der Klis M., eds, *Compact Stellar X-ray Sources*. Cambridge Univ. Press, Cambridge, p. 547
 Woods P. M., Kouveliotou C., Göğüs E., Finger M. H., Swank J., Smith D. A., Hurley K., Thompson C., 2001, *ApJ*, 552, 748
 Woods P. M., Kouveliotou C., Göğüs E., Finger M. H., Swank J., Markwardt C. B., Hurley K., van der Klis M., 2002, *ApJ*, 576, 381
 Woods P. M. et al., 2004, *ApJ*, 605, 378
 Yakovlev D. G., Pethick C. J., 2004, *ARA&A*, 42, 169
 Yakovlev D. G., Kaminker A. D., Gnedin O. Y., Haensel P., 2001, *Phys. Rep.*, 354, 1

This paper has been typeset from a $\text{\TeX}/\text{\LaTeX}$ file prepared by the author.